Quantum Complexity
(WORK IN PROGRESS)

Amey Gaikwad
Department of Physics, Indian Institute of Technology, Bombay

Work started in May 2018 at Swansea University under the guidance of Dr.S.Prem Kumar

Contents

1 Circuit Complexity

The notion of complexity we are trying to implement has been borrowed from MYERS. Complexity theory is a well defined notion in computer science. Given

an initial sequence of bits and a final sequence of bits. Each bit can take two values. Using just the switching operator, what is the minimum number of operations that are required to go from one sequence to the other ? This minimum value is complexity. In MYERS, the authors have tried to implement an analogous technique for quantum harmonic oscillators.

Motivation to study complexity.....

2 Complexity of simple harmonic oscillators

Consider the case of a single harmonic oscillator. Given a reference state

$$\psi_R(x) = \sqrt{\frac{\omega_0}{\pi}}\exp(-\frac{\omega_0 x^2}{2}) \tag{1}$$

and a target state

$$\psi_T(x) = \sqrt{\frac{\omega}{\pi}}\exp(-\frac{\omega^2 x^2}{2}) \tag{2}$$

and only the operator

$$U = \exp(ixp) \tag{3}$$

the depth of the circuit is given by the number of operations required to connect ψ_R and ψ_T. Now, there exists a minimum way of doing this. The minimum number of operations required to connect these two states is defined as the complexity of the quantum theory. In the above case, the complexity is given by:

$$C = \frac{1}{2}\left|\ln\left(\frac{\omega_1}{\omega_0}\right)\right| \tag{4}$$

Similarly for N oscillators, the complexity can be calculated to be

$$C = \frac{1}{2}\sqrt{\sum_{k=0}^{N-1}\log^2\left(\frac{\omega_k}{\omega_0}\right)} \tag{5}$$

Here ω_0 is the frequency of the N oscillators in the reference state, while ω_k is the frequency of the k^{th} oscillator in the target state. The derivation of the above expression is given in (REFER MYERS).

3 Complexity in QFT

Complexity in QFT... generalize to d dimensions. The result of the complexity calculation in the previous section can be extended to an infinite number if harmonic oscillators which in turn changesthe summation to an integral.

4 Time dependent frequency

In this section we consider the case of an harmonic oscillator with a time dependent frequency. Consider the Schrodinger's equation for a harmonic oscillator with a time dependent frequency:

$$i\frac{\partial\psi}{\partial t} = -\frac{1}{2}\frac{\partial^2\psi}{\partial x^2} + \frac{1}{2}\omega^2(t)x^2\psi \tag{6}$$

Consider the following ansatz for the wave function:

$$\psi = \exp\Big[-i\int_0^t dt'\frac{A(t')}{2}\Big]\exp\Big[-\frac{A(t)x^2}{2}\Big] \tag{7}$$

Therefore:

$$\begin{aligned} i\dot{\psi} = \frac{A(t)}{2}\exp\Big[-i\int_0^t dt' A(t')/2\Big]\exp\Big[-\frac{A(t)x^2}{2}\Big] \\ -i\frac{\dot{A}(t)}{2}x^2\exp\Big[-i\int_0^t dt' A(t')/2\Big]\exp\Big[-\frac{A(t)x^2}{2}\Big] \end{aligned} \tag{8}$$

and

$$\begin{aligned} \psi'(x) &= -A(t)x\cdot\exp\Big[-i\int_0^t dt' A(t')/2\Big]\exp\Big[-\frac{A(t)x^2}{2}\Big] \\ \psi''(x) &= -A(t)\exp\Big[-i\int_0^t dt' A(t')/2\Big]\exp\Big[-\frac{A(t)x^2}{2}\Big] \\ &+ A^2(t)x^2\exp\Big[-i\int_0^t dt' A(t')/2\Big]\exp\Big[-\frac{A(t)x^2}{2}\Big] \end{aligned} \tag{9}$$

Using this ansatz and plugging the above relations in (6), we get the following Riccati equation for $A(t)$:

$$i\dot{A(t)} = A^2(t) - \omega^2(t) \tag{10}$$

If we use the following substitution:

$$A(t) = -i\frac{\dot{\phi^*}(t)}{\phi^*(t)} \tag{11}$$

Hence (10) transforms to the following:

$$\ddot{\phi}(t) + \omega^2(t)\phi(t) = 0 \tag{12}$$

Hypothesis:
I believe that in the context of complexity, the normalisation factor will not play a role. Once a function has been normalised for a given time, it will remain normalised for all future times. The normalisation constant depends

on the the value of $A(t)$. It does not add any extra degree of freedom to the problem. The analysis that takes place in the following sections takes into account the hypothesis that the complexity only depends on the width of the harmonic oscillator, i.e $A(t)$. By assuming this hypothesis, we can easily adopt the procedure used in the case of quantum field theory in Minkowski space, which is exactly what will be done in the coming sections.

5 dS_3 - Conformal Time

Now we calculate the complexity for a quantum field theory in de-Sitter space in the conformal frame. The Lagrangian density under consideration is the following:

$$L_E = \frac{R^3}{2}\Big[R^{-2}(\partial_\tau \Phi_E)^2 - R^{-2}(\nabla_{S^2}\Phi_E)^2 - \Big(\frac{M_0^2}{\cos^2(\tau)} + \frac{1}{4R^2}\Big)\Big] \tag{13}$$

We define the canonical momentum as:

$$\Pi_E = -\sqrt{|\det g|}g^{0\mu}\partial_\mu \Phi = R\dot{\Phi} \tag{14}$$

Defining this way leads to the following commutation relation:

$$[\Phi_E(x,t), \Pi_E(y,t)] = i\hbar\delta(x-y) \tag{15}$$

Hence the Hamiltonian is given by:

$$H_E = \int_{S^2} \frac{1}{2}\Big[\frac{\Pi^2}{R^2} + (\nabla_{S^2}\Phi_E)^2 + \Big(\frac{M_0^2R^2}{\cos^2(\tau)} + \frac{1}{4}\Big)\Big]d^2\Omega \tag{16}$$

Now we perform the following mode decomposition:

$$\Phi_E = \frac{1}{\sqrt{R}}\sum_{l=0}^{\infty}\sum_{m=-l}^{m=l}\Big[a_{lm}Y_l^m(\Omega)C_l(\tau) + a_{lm}^\dagger Y_l^{m*}(\Omega)C_l^*(\tau)\Big] \tag{17}$$

where Ω covers S^2 and Y_l^m are the spherical harmonic modes. Using this mode decomposition, we get the following form of the Hamiltonian:

$$H_E = \sum_l (2l+1)\frac{1}{2}\Big[\frac{\Pi_E^2}{R^2} + \Big((l+\frac{1}{2})^2 + \frac{M^2R^2}{\cos^2(\tau)}\Big)\Phi_E^2\Big] \tag{18}$$

Then we can construct the Schrodinger's equation so as to get the nature of the wave function we are dealing with. Therefore, considering just one mode, we get the following equation to be satisfied by the wave function ($R = 1$):

$$i\dot{\Psi}_E = -\frac{1}{2}\frac{d^2\Psi_E}{dx^2} + \frac{1}{2}\Big(l(l+1) + \frac{M_0^2}{\cos^2(\tau)}\Big)x^2\Psi_E \tag{19}$$

This equation looks like the equation for an oscillator with a time dependent frequency $\omega(t)$.

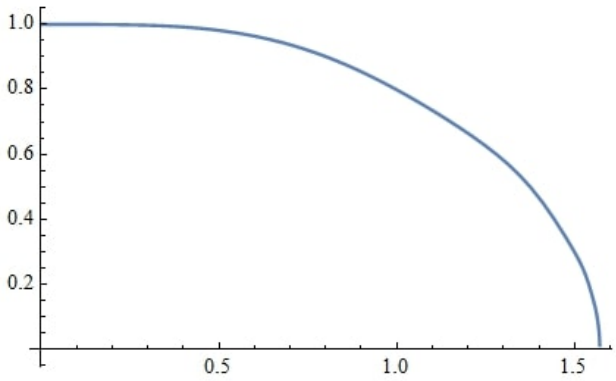

Figure 1: $|\phi_{l_E}|$ for $l = 1$

5.1 Complexity

We are interested in adopting the method as described by MYERS to free field theories in de Sitter space in the conformal frame. By inspecting (18) we deduce that in the conformal frame the time dependent frequency $\omega_E(\tau)$ is given by the following:

$$\omega_E^2(\tau) = l(l+1) + M_0^2 \sec^2(\tau) \tag{20}$$

Therefore from (12), we get the following differential equation:

$$\ddot{\phi}_{l_E}(\tau) + \omega_E^2(\tau)\phi_{l_E}(\tau) = 0 \tag{21}$$

For getting an idea of how these functions behave we need to set a tolerance value ϵ so as to probe between the time limits 0 and $\pi/2-\epsilon$. We use the following tolerance value for our calculations:

$$\epsilon = 0.01 \tag{22}$$

Now we can analyse (21) to get an idea of how ϕ_l behaves. The graph (1 is where we have plotted the nature of $|\phi_{l_E}|$ for $l = 1$. The mathematical structure of ϕ_1 comprises the summation of two hypergeometric functions. We now mention some general properties of $|\phi_{l_E}(\tau)|$.

- The graph for all values of l remains constant over the majority of the interval between 0 and $\pi/2 - \epsilon$
- As the value of l increases, the cutoff beyond which the function starts monotonically decreasing. also increases.
- As the value of l increases, the minimum value also increases but the maximum value remains constant at 1.

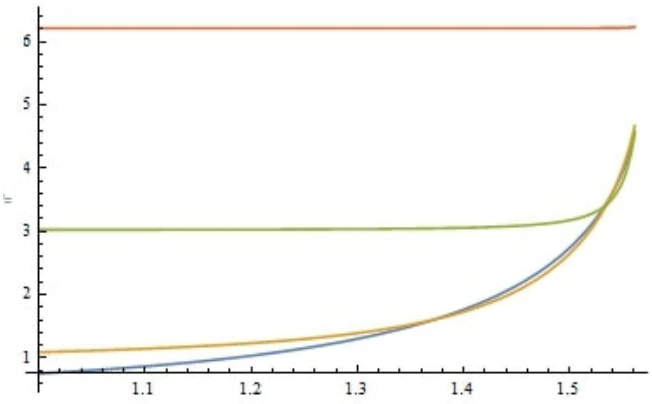

Figure 2: Graphs for l=1,2,20,200 $A_l(\tau)$

After this, we get an expression for $A_l^E(\tau)$ for each mode. In the graph, (2), the nature of A_l are plotted for 4 values of l with the highest value of l corresponding to the highest value in the graph. Some properties concerning the behaviour of $|A_l(\tau)|$:

- Minimum value increases with l
- Remains constant and beyond a specific time, starts monotonically increasing.
- The cutoff beyond which it starts increasing remains approximately the same.

Now each value of l has a degeneracy of the order $(2l+1)$.Therefore, our formula for complexity as adopted from QFT is given by the following:

$$2C_E = \sqrt{\sum_{l=0}^{\infty}(2l+1)|\ln^2 A_l(\tau)|} \tag{23}$$

where we have assumed that the reference state frequency is time independent and will contribute a finite amount.The complexity for each mode get added up in quadrature to give the complexity for the system. We can neglect the reference term and focus on the above expression. Now, we solve for ϕ_E with the following initial conditions:

$$\begin{aligned} \phi_{l_E}(0) &= 1 \\ \phi'_{l_E}(0) &= i(l(l+1)+M_0^2) \end{aligned} \tag{24}$$

We also need to fix the value of M_0. In the calculation done below, we have set it to 1. The summation over all the modes would not be numerically solvable.There

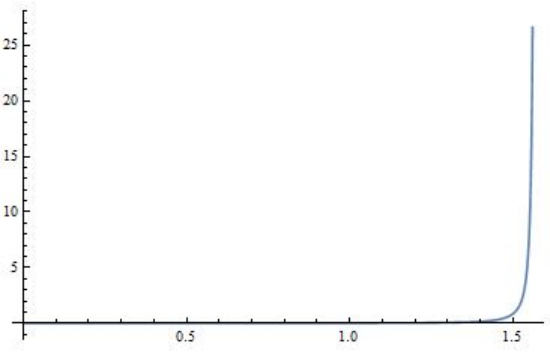

Figure 3: $C_E(\tau) - C_E(0)$

are two types of cutoff - comoving and physical. The physical cutoff $\Lambda_{\text{physical}}$ is a fixed high number while the comoving cutoff $\Lambda_{\text{comoving}}$ changes with time. They are related in the following way:

$$\Lambda_{\text{comoving}} = \frac{\Lambda_{\text{physical}}}{\cos(\tau)} \tag{25}$$

We fix the physical cutoff to some large value.The large value is fixed so that the $l(l+1) > \sec(\tau)$ for all times from 0 to $\pi/2 - \epsilon$ where ϵ has been defined in (22).The reason for this will be clear when we define what we mean to be UV and IR modes.

Now, we can proceed with the calculation for complexity.

5.2 $C_E(\tau) - C_E(0)$

Following summation needs to be performed:

$$C_E(\tau) = \sum_{l=0}^{\Lambda_{\text{physical}}} \sqrt{(2l+1)|\ln^2 A_l(\tau)|} \tag{26}$$

Here $\Lambda_{\text{physical}} = 700$. The graph remains almost constant and then shows a steep increase. In graph (3), we plot the variation of the complexity with variation in conformal time. As is clear from the graph, the complexity remains constant predominantly, and then near $\pi/2$, it increases steeply.

We also need to find out the exact behaviour of the divergences. To this end, we first plot the variations of the infrared and ultraviolet segments of the modes with conformal time. Our definition of ultraviolet is given as follows:

$$(l + \frac{1}{2})^2 > M_0^2 \sec^2(\tau) \tag{27}$$

The mode numbers which satisfy the above condition fall in the bracket of ultraviolet modes. The others are defined to be the infrared modes.

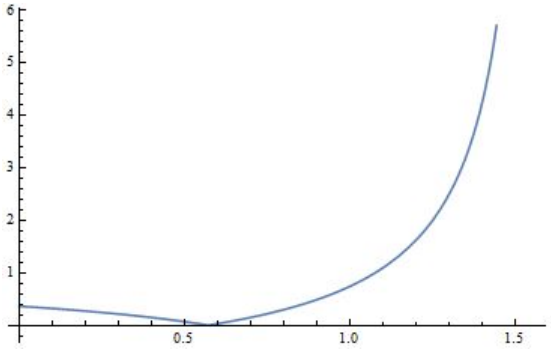

Figure 4: Theoretical estimate for IR contribution to complexity

5.3 Infrared contribution

We first try to predict the behaviour of the infrared modes and then corroborate our prediction with a numerical analysis.

5.3.1 Theoretical

So, consider the equation (12). If $\omega(\tau)$ varies as τ^{-2}, then $\phi(\tau)$ varies as $1/\sqrt{\tau}$. This can be easily checked. Now, coming back to equation (21), we see that $\omega_E(\tau)$ satisfies this condition. This is because of the following behaviour near $\pi/2$:

$$\sec(\tau) \approx \frac{1}{\pi/2 - \tau} \tag{28}$$

The above approximation will hold for the infrared modes because near $\pi/2$, (39) will be reversed due to the large value of $\sec(\tau)$. Therefore, the infrared contribution to the $4C_E^2$ can be given by the following expression:

$$\sum_{l=1}^{[m \sec t]} (2l+1) |\ln A_l(t)|^2 \tag{29}$$

Using the following approximation,

$$|\ln A_l(t)|^2 \approx \ln^2 (\pi/2 - t) \tag{30}$$

we get the infrared contribution as:

$$4C_E^2(\tau) \approx \frac{m}{(\pi/2 - t)} \ln^2 (\pi/2 - t) \tag{31}$$

In plot (4), we have shown the variation of the estimate (31) with time.

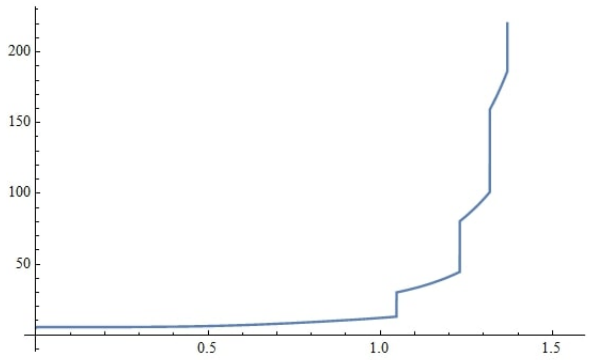

Figure 5: Numerical estimate for the IR contribution to the complexity.

5.3.2 Numerical

Here we calculate the numerical estimate for the IR contribution to the complexity. The graph is given by (5). As we can see from the graphs (5) and (4), the late time behaviour near $\pi/2$ is approximately the same. This corroborates our theoretical guess that the IR contribution to the complexity squared does behave in the manner given by (31).

5.4 Ultraviolet Contribution

For analysing the ultraviolet modes, we perform a numerical analysis for calculating their contribution. The UV contribution to $4C_E^2$ is given by the following :

$$\sum_{[m \sec t]}^{l_{\text{upper}}} (2l+1) |\ln A_l(t)|^2 \tag{32}$$

Since we are summing over the UV modes, the lower cutoff for the mode number will be :

$$l_{\text{lower}} = M_0[\sec(\tau)] \tag{33}$$

The upper cutoff can again be physical or the comoving cutoff. The reason for having two cutoffs is that while the definition for physical momentum seems to be consistent with our criteria for UV modes, the comoving cutoff serves as a better segue for defining UV modes - it serves as a more accurate description of what is UV and what is infrared. Through the physical cutoff, the number of UV modes decreases with time. On the other hand, using the comoving cutoff, the number of UV modes does not decrease with time since the upper limit is also dynamic. Now, we state the results:

- If we use the $\Lambda_{\text{physical}}$ as l_{upper} then the complexity decreases near $\pi/2$ after remaining almost constant. Refer graph (7).

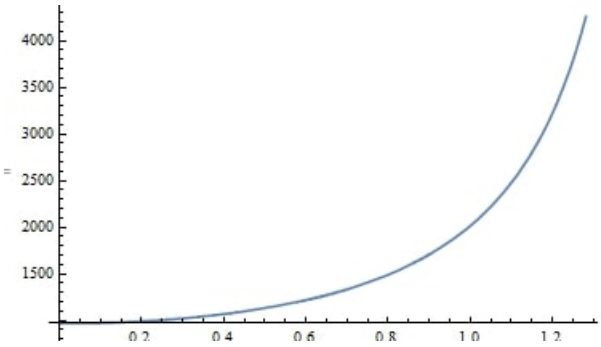

Figure 6: UV contribution to complexity with $l_{\text{upper}} = \Lambda_{\text{comoving}} = [200\text{sec}(\tau)]$

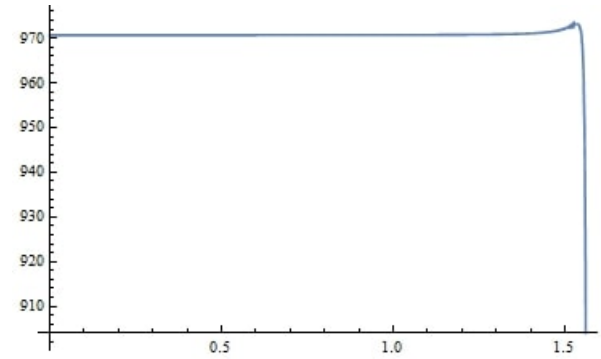

Figure 7: UV contribution to complexity with $l_{\text{upper}} = \Lambda_{\text{physical}} = 200$

- If we use $\Lambda_{\text{comoving}}$ as l_{upper} then the complexity increases. Refer graph (6) .

There exists a neat reason why we encounter these two very different outcomes. When we use $\Lambda_{\text{physical}}$ for l_{upper} as time progresses, the UV modes quickly turn into infrared modes according to our definition of what UV/ Infrared entails as given by (39).Hence as time progresses, the complexity decreases as the number of contributing modes decreases at a faster rate than the rate of increase in complexity of each individual mode.

5.5 WKB approximation

To perform a theoretical analysis of how the UV modes behave, we perform WKB approximations. This is because in the large l limit, we can neglect the $m\text{sec}(\tau)$ contribution to the time dependent frequency. We employ this method twice - zeroth order approximation and a higher order WKB approximation.

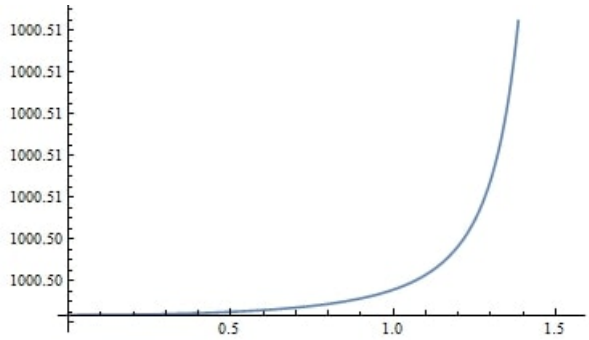

Figure 8: $\phi_l(\tau)$ via the WKB approximation with $m = 1$ and $l = 10$

5.5.1 Zeroth Order approximation

We will also compare the nature of $\phi_l(\tau)$ with variation in conformal time between the numerical calculation performed in section (5.1) and the WKB approximation. We use the following ansatz for the solution to (12):

$$\phi(\tau) = \frac{C}{\sqrt{p(\tau)}} \exp\Big[-i \int_0^\tau dt p(t) \Big] \tag{34}$$

where

$$p(\tau) = ((l + \frac{1}{2})^2 + M_0^2 \sec^2(\tau))^{1/2} \tag{35}$$

In graph (8), we show the variation of $A_l(\tau)$ with variation in the conformal time. The variation of $\phi_l(\tau)$ very well with the graph obtained via exact numerical calculations in section (5.1). To see how closely the two plots match, graph (9) shows that the two curves follow each other very closely. This shows that the WKB approximation matches nicely with the exact numerical results and can be used for describing the variation of complexity with conformal time.

Once we have this ansatz for $\phi(\tau)$, we solve for $A_l(\tau)$ with the help of (11) and again we solve for the complexity given by:

$$4C_{wkb}^2 = \sum_{[m \sec \tau]}^{[\Lambda_{\text{comoving}}]} (2l+1) |\ln A_l(\tau)|^2 \tag{36}$$

Via the zeroth order approximation the graph of complexity is given by 10. Here the upper cutoff is the physical cutoff ($\Lambda_{\text{physical}} = 100$).

In the following section we improve our precision of doing the WKB approximation since we are interested in the UV divergent terms contributing to the complexity.While the zeroth order WKB was good enough, to get a handle on the variation of the divergent terms, we need to be as precise as we could be. Hence we resort to the higher order WKB approximation.

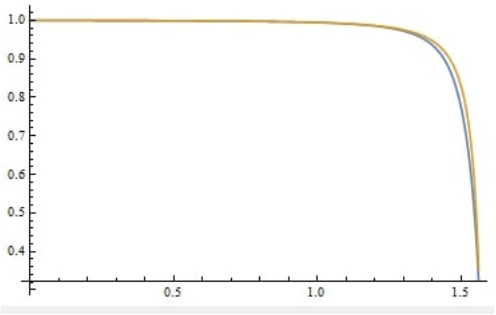

Figure 9: Comparison between the nature of $\phi_l(\tau)$ - the WKB and the numerical results

.

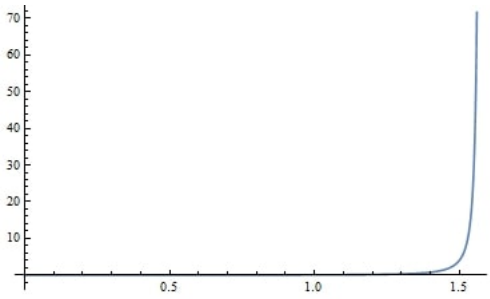

Figure 10: Complexity $C_{\text{wkb}}(\tau) - C_{\text{wkb}}(0)$ with $l_{\text{upper}} = \Lambda_{\text{physical}} = 100$ for the zeroth order WKB approximation

.

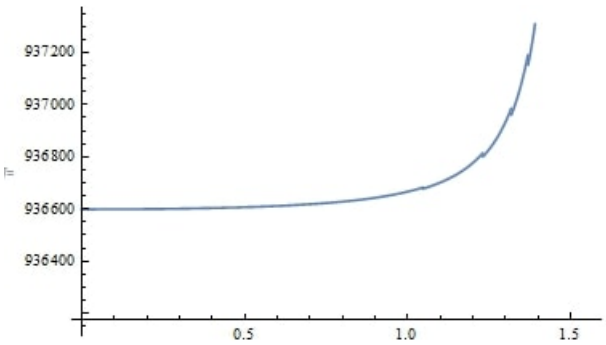

Figure 11: Complexity - higher order WKB approximation with$\Lambda = \Lambda_{\text{physical}} = 200$

.

5.5.2 Higher Order WKB

We do the WKB analysis by considering corrections to the $p(\tau)$ term. Therefore the ansatz remains the same as above with the following expression for $p(\tau)$:

$$p(\tau) = \sqrt{\left(\omega_0(\tau) + \frac{3}{4}\cdot\frac{\omega_0'(\tau)}{\omega_0^2(\tau)} - \frac{1}{2}\cdot\frac{\omega_0''(\tau)}{\omega_0(\tau)}\right)} \tag{37}$$

where

$$\omega_0(\tau) = ((l+\frac{1}{2})^2 + M_0^2\text{sec}^2(\tau))^{1/2} \tag{38}$$

where again we assign $M_0 = 1$.

Now, using this expression we find the approximate ultraviolet contribution to the complexity.The contribution in general will depend on Λ, m and τ.Here Λ can be $\Lambda_{\text{physical}}$ or $\Lambda_{\text{comoving}}$ depending on our choice of l_{upper}. In the UV limit and after approximating the summation as an integral, we get the following UV approximation to $4C^2(\tau)$:

$$\begin{aligned} \tilde{\Lambda} &= (\Lambda + \frac{1}{2})^2 \\ \zeta &= (\lfloor m\sec t\rfloor + \frac{1}{2})^2 \end{aligned} \tag{39}$$

$$\begin{aligned} 4C_{UV}^2 =& \frac{1}{4}\Big[\tilde{\Lambda}\ln^2\tilde{\Lambda} - 2\tilde{\Lambda}\ln\tilde{\Lambda} + 2\tilde{\Lambda} - \zeta\ln^2\zeta + 2\zeta\ln\zeta - 2\zeta\Big] + \\ & \frac{1}{4}\cdot m^2\text{sec}^2(t)\cdot(\ln^2\tilde{\Lambda} - \ln^2\zeta) \end{aligned} \tag{40}$$

Nature of complexity graph is the same numerically and theoretically for the whole spectrum but not the same when only the UV modes are considered. Theoretically, via the WKB approximation, the complexity increases irrespective of

our choice of $\Lambda_{\text{physical}}$ or $\Lambda_{\text{comoving}}$ for Λ. Refer graph (11) for the contribution of the UV modes to $4C^2$ given by equation (**??**). The increase is reminiscent of the graph that we had obtained via a numerical analysis in section (5.4).

6 Global time

The metric is given by:

$$ds^2 = -dt^2 + R^2\cosh^2\Big(\frac{t}{R}\Big)d\Omega_2^2 \tag{41}$$

The Lagrangian density is given by:

$$L_G = R^2\cosh^2\Big(\frac{t}{R}\Big)\Big[\frac{1}{2}(\partial_t\Phi_G)^2 - \frac{1}{2R^2}\text{sech}^2\Big(\frac{t}{R}\Big)(\nabla_{S^2}\Phi_G)^2 - \frac{1}{2}\Big(M_0^2+\zeta R\Big)\Phi_G^2\Big] \tag{42}$$

The canonical momentum is given by (14):

$$\Pi_G = R^2\cosh^2\Big(\frac{t}{R}\Big)\partial_t\Phi_G \tag{43}$$

so as to satisfy the commutation relation as given by (15). Then we get the following Hamiltonian:

$$H_G = \int_{S^2}\frac{1}{2}\Big[\frac{\Pi_G^2}{R^2\cosh^2(t/R)} + (\nabla_{S^2}\Phi_G)^2 + (M_0^2+\zeta R)R^2\cosh^2(t/R)\Phi_G^2\Big] \tag{44}$$

We employ the following mode decomposition:

$$\Phi_G = \frac{1}{\sqrt{R}}\sum_{l=0}^{\infty}\sum_{m=-l}^{m=l}\Big[a_{lm}Y_l^m(\Omega)D_l(t) + a_{lm}^\dagger Y_l^{m*}(\Omega)D_l^*(t)\Big] \tag{45}$$

We rewrite the Hamiltonian with $R=1$ in terms of this mode decomposition to get:

$$H_G = \sum_{l=0}^{\infty}(2l+1)\frac{1}{2}\Big[\frac{\Pi_G^2}{\cosh^2(t)} + (l(l+1) + M_0^2\cosh^2(t))\Big] \tag{46}$$

Similar to the conformal frame case, we get the following Schodinger equation considering just one mode:

$$i\dot{\Psi}_G = -\frac{1}{2}\frac{d^2\Psi_G}{d\tilde{x}^2}\frac{1}{\cosh^2(t)} + \Big(l(l+1) + M_0^2\cosh^2(t)\Big)\tilde{x}^2\Psi_G \tag{47}$$

(47) is different from the usual Schrodinger equation of an oscillator with a time dependent frequency. If we perform the following coordinate re-definitions, we can connect (47) and (19).

$$\begin{aligned}\cos(\tau) &= \frac{1}{\cosh(t)}\\ \tilde{x} &= \frac{x}{\sqrt{\cos(\tau)}}\end{aligned} \tag{48}$$

Hence if we calculate the wave function in the conformal frame, we can easily get the wavefunction in the global frame by employing (48). So in the global coordinates

$$A_{l_G}(t) = \frac{A_{l_E}(\tau(t)))}{\cos(\tau)} \tag{49}$$

Hence again we find that A_{l_G} will also increase with time which in turn implies that the complexity increases with time. To find the nature of the divergent terms in global coordinates we just use the coordinate transformation (48).

7 Holographic calculation

We consider the metric of a topological crunch AdS model given by:

$$ds^2 = -(1+r^2)d\tau^2 + \frac{dr^2}{1+r^2} + r^2 d\Omega_2^2 + (1+r^2)\cos^2(\tau)d\phi^2 \tag{50}$$

We are interested in calculating the volume of the extremal surface at constant τ at the boundary. We then wish to study how this volume varies as the boundary conditions are varied. Volume of a surface is given by:

$$V = \int d^d\sigma \sqrt{det(*g_{\Sigma_t})} \tag{51}$$

where $*g$ is the pullback metric and Σ_t is the surface under consideration. The time variable τ will be a function just of the radial coordinate $\tau(r)$ with the boundary condition being

$$\lim_{r\to\infty} \tau(r) = \tau_b \tag{52}$$

Therefore, the pullback metric will be

$$ds^2 = dr^2\Big[\frac{1}{1+r^2} - (1+r^2)(\frac{d\tau}{dr})^2\Big] + r^2 d\Omega_2^2 + \cos^2(\tau)(1+r^2)d\phi^2 \tag{53}$$

Using the above relations, the expression for the volume is given by:

$$V = 8\pi \int dr r^2 \cos(\tau(r))\Big[1 - (1+r^2)^2\Big(\frac{d\tau}{dr}\Big)^2\Big]^{1/2} \tag{54}$$

Since we are interested in finding the extremal surface, we need to extremize the volume as given above. Therefore, we use the Euler Lagrange equation to solve it in order to get $\tau(r)$ which we plug back in (54) to get the volume of the extremal surface. We use the following two boundary conditions:

$$\begin{aligned} \tau(\infty) &= \tau_b \\ \tau'(0) &= 0 \end{aligned} \tag{55}$$

The second condition is necessary in order to have no kinks near the $r = 0$ region.

The integral (54) does not converge. So we need to interest ourselves with the nature of the divergent terms. In order to do this we expand $\tau(r)$ around infinity in the following manner:

$$\tau(r) = \tau_b + \frac{c_1}{r} + \frac{c_2}{r^2} + \frac{c_3}{r^3} + \frac{c_4}{r^4} + ... \tag{56}$$

If we expand the integrand of (54), around infinity and substitute (56), we can calculate the coefficients and the nature of divergences.We get the following results:

$$\begin{aligned} c_1 &= c_3 = c_5 = 0 \\ c_2 &= -\frac{1}{6}\tan(\tau_b) \\ c_4 &= \frac{45}{216}\tan(\tau_b) + \frac{7}{216}\tan^3(\tau_b) \end{aligned} \tag{57}$$

We can also conclude that the divergent terms of the integral (54) depend only on c_2 and c_4. So the higher order terms need not be calculated. The exact behaviour of the divergent terms contributing to the volume is given by:

$$\frac{1}{3}\cos(\tau_b)\Lambda^3 + \frac{1}{9}\sin(\tau_b)\tan(\tau_b)\Lambda \tag{58}$$

We subtract out the divergent piece from the integrand so as to obtain the finite contribution to study the variation of the volume of the minimal surface with variation in time. Once we have the nature of how the divergent part of the integral behave, we can resort to numerical techniques to calculate the volume. We use the following boundary values:

$$\begin{aligned} \tau'(0.01) &= 0.000001 \\ \tau(0.01) &= \tau_0 \end{aligned} \tag{59}$$

to evaluate the integral from 0.000001 to 100. We get the data as tabulated in 7. We see in figure (12) that with time the volume decreases.The nature of $\tau(r)$ with respect to r changes when we change τ_0 from 1.047 to 1.05. This is because near these initial values, the value of τ_b approaches $\pi/2$.

If we multiply our data points with $\cos(\tau)$, we get an approximately linear decreasing graph. Therefore, we can estimate that the volume decreases like $1/(\pi/2 - \tau)$.

8 Scalar sector SYM

The space under consideration is $dS_3 \times S_1$.

$$L = \frac{1}{2}\Big[(\partial_\tau \Phi)^2 - (\nabla_{S^2}\Phi)^2 - \frac{(\partial_\psi \Phi)^2}{\cos^2(\tau)} - \Big(\frac{1}{4R^2}\Big)\Phi^2\Big] \tag{60}$$

V (finite part)	τ_0	τ_b
-0.0793232	0.1	0.117875
-0.320804	0.2	0.236195
-0.735929	0.3	0.355458
-1.34744	0.4	0.476274
-2.19692	0.5	0.599471
-3.36206	0.6	0.726273
-5.00073	0.7	0.85868
-7.4884	0.8	1.00039
-12.0296	0.9	1.15974
-27.2069	1.0	1.36584
-91.1167	1.04	1.50459
-705.521	1.047	1.56005

Table 1: Variation of volume with variation in τ_b

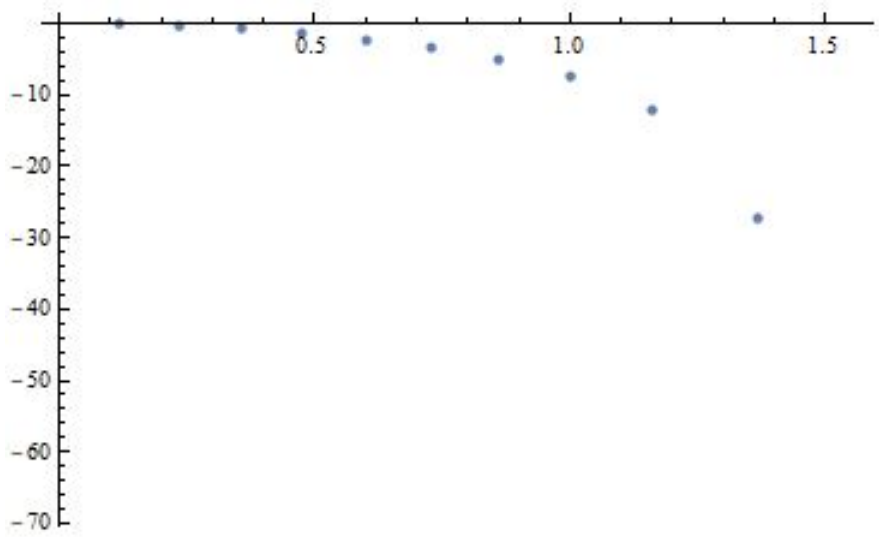

Figure 12: Variation of the minimal surface with constant $\tau = \tau_b$ at the boundary, with variation in τ_b

.

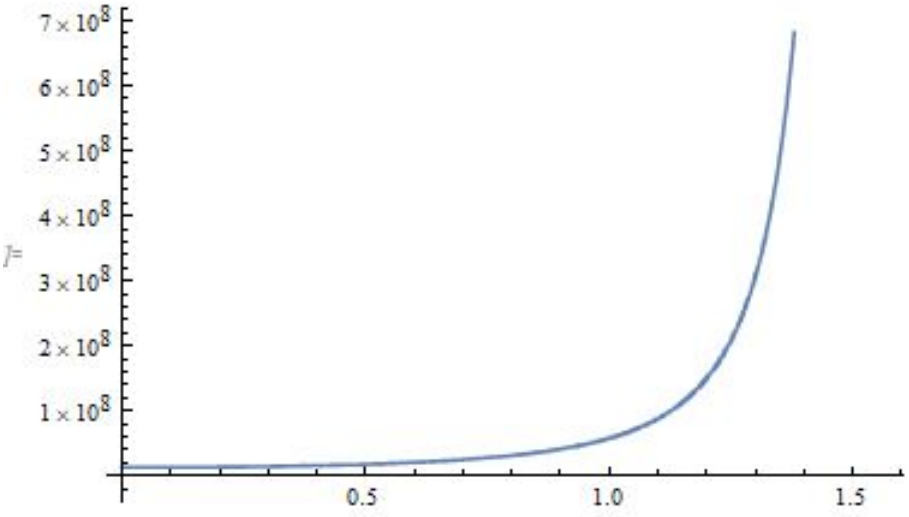

Figure 13: Variation of the complexity for the scalar sector of the SYM model

.

The metric under consideration is given by:

$$ds^2 = \frac{1}{\cos^2(\tau)}(-d\tau^2 + d\Omega_2^2) + d\psi^2 \tag{61}$$

where ψ parametrizes the compactified circle S_1. After mode decomposition, we get the following expression for the Hamiltonian:

$$H = \sum_{l=0}^{\infty}\sum_{n=0}^{\infty} 2(2l+1)\frac{1}{2}\left[\Pi^2 + \left((l+1)^2 + \frac{n^2}{\cos^2(\tau)}\right)\Phi^2\right] \tag{62}$$

We now need to calculate the complexity for this system. The method follows a similar method to section (5). However, now we have two cutoff parameters - one for each summation. On superficial examination, it can be guessed that in this case too, the complexity is going to increase since the "mass term" also increases with each iteration. In equation (18), the mass term is constant. In equation (62) however, the "mass" term varies from 0 to ∞ due to the Fourier decomposition due to the extra compactified circle present in the geometry. The graph for the increase has been plotted in (13).

Now, we analyse the nature of divergence arising due to the UV modes in a manner similar to the WKB approximation we employed for the earlier case. The answer will depend on two cutoffs. Referring to the earlier formulae (39) and (40), we get the UV contribution to the complexity in (63). If Γ represents the

cutoff for the Fourier modes (corresponding to the modes along the compactified circle), with the definitions for $\tilde{\Lambda}$ and ζ remaining the same as before:

$$\text{In Progress} \tag{63}$$

We have mentioned the contribution only upto the Γ^2 order. Due to the polylog variation of the complexity squared, we have all the orders of Γ appearing in the expansion.

References

[1] Jose L. F. Barbon and Eliezer Rabinovici. "Holographic complexity and spacetime singularities". In: *JHEP* 01 (2016), p. 084. DOI: 10.1007/JHEP01(2016)084. arXiv: 1509.09291 [hep-th].

[2] Arpan Bhattacharyya, Arvind Shekar, and Aninda Sinha. "Circuit complexity in interacting QFTs and RG flows". In: *JHEP* 10 (2018), p. 140. DOI: 10.1007/JHEP10(2018)140. arXiv: 1808.03105 [hep-th].

[3] Daniel Boyanovsky, Hector J. de Vega, Richard Holman, S. Prem Kumar, and Robert D. Pisarski. "Nonequilibrium evolution of a 'Tsunami': Dynamical symmetry breaking". In: *Phys. Rev.* D57 (1998), pp. 3653–3669. DOI: 10.1103/PhysRevD.57.3653. arXiv: hep-ph/9711258 [hep-ph].

[4] Adam R. Brown, Daniel A. Roberts, Leonard Susskind, Brian Swingle, and Ying Zhao. "Complexity, action, and black holes". In: *Phys. Rev.* D93.8 (2016), p. 086006. DOI: 10.1103/PhysRevD.93.086006. arXiv: 1512.04993 [hep-th].

[5] Adam R. Brown, Daniel A. Roberts, Leonard Susskind, Brian Swingle, and Ying Zhao. "Holographic Complexity Equals Bulk Action?" In: *Phys. Rev. Lett.* 116.19 (2016), p. 191301. DOI: 10.1103/PhysRevLett.116.191301. arXiv: 1509.07876 [hep-th].

[6] Adam R. Brown and Leonard Susskind. "Second law of quantum complexity". In: *Phys. Rev.* D97.8 (2018), p. 086015. DOI: 10.1103/PhysRevD.97.086015. arXiv: 1701.01107 [hep-th].

[7] Josiah Couch, Stefan Eccles, Ted Jacobson, and Phuc Nguyen. "Holographic Complexity and Volume". In: *JHEP* 11 (2018), p. 044. DOI: 10.1007/JHEP11(2018)044. arXiv: 1807.02186 [hep-th].

[8] Lucas Hackl and Robert C. Myers. "Circuit complexity for free fermions". In: *JHEP* 07 (2018), p. 139. DOI: 10.1007/JHEP07(2018)139. arXiv: 1803.10638 [hep-th].

[9] Ro Jefferson and Robert C. Myers. "Circuit complexity in quantum field theory". In: *JHEP* 10 (2017), p. 107. DOI: 10.1007/JHEP10(2017)107. arXiv: 1707.08570 [hep-th].

[10] S. Prem Kumar and Vladislav Vaganov. "Nonequilibrium dynamics of the O(N) model on dS_3 and AdS crunches". In: *JHEP* 03 (2018), p. 092. DOI: 10.1007/JHEP03(2018)092. arXiv: 1802.08202 [hep-th].

[11] S. Prem Kumar and Vladislav Vaganov. "Probing crunching AdS cosmologies". In: *JHEP* 02 (2016), p. 026. DOI: 10.1007/JHEP02(2016)026. arXiv: 1510.03281 [hep-th].

[12] Leonard Susskind. "Entanglement is not enough". In: *Fortsch. Phys.* 64 (2016), pp. 49–71. DOI: 10.1002/prop.201500095. arXiv: 1411.0690 [hep-th].

[13] Leonard Susskind. "PiTP Lectures on Complexity and Black Holes". In: 2018. arXiv: 1808.09941 [hep-th].

[14] Leonard Susskind. "Three Lectures on Complexity and Black Holes". In: 2018. arXiv: 1810.11563 [hep-th].